How to cite: *Angew. Chem. Int. Ed.* **2022,** *61,* e202205575
International Edition: doi.org/10.1002/anie.202205575
German Edition: doi.org/10.1002/ange.202205575

Defluorination Reactions

Light-Driven Hydrodefluorination of Electron-Rich Aryl Fluorides by an Anionic Rhodium-Gallium Photoredox Catalyst

*James T. Moore[+], Michael J. Dorantes[+], Zihan Pengmei, Timothy M. Schwartz, Jacob Schaffner, Samantha L. Apps, Carlo A. Gaggioli, Ujjal Das, Laura Gagliardi, David A. Blank, and Connie C. Lu**

Abstract: An anionic Rh–Ga complex catalyzed the hydrodefluorination of challenging C–F bonds in electron-rich aryl fluorides and trifluoromethylarenes when irradiated with violet light in the presence of H_2, a stoichiometric alkoxide base, and a crown-ether additive. Based on theoretical calculations, the lowest unoccupied molecular orbital (LUMO), which is delocalized across both the Rh and Ga atoms, becomes singly occupied upon excitation, thereby poising the Rh–Ga complex for photoinduced single-electron transfer (SET). Stoichiometric and control reactions support that the C–F activation is mediated by the excited anionic Rh–Ga complex. After SET, the proposed neutral Rh^0 intermediate was detected by EPR spectroscopy, which matched the spectrum of an independently synthesized sample. Deuterium-labeling studies corroborate the generation of aryl radicals during catalysis and their subsequent hydrogen-atom abstraction from the THF solvent to generate the hydrodefluorinated arene products. Altogether, the combined experimental and theoretical data support an unconventional bimetallic excitation that achieves the activation of strong C–F bonds and uses H_2 and base as the terminal reductant.

Introduction

Organofluorines are ubiquitous in today's society due to their unique characteristics, such as increased thermal stability and lipophilicity, and are prevalent in agrochemicals (≈30 %) and pharmaceuticals (≈10 %).[1] However, their extended lifetimes and toxicity, particularly as perfluorocarbons, motivate efforts to develop processes capable of cleaving the C–F bond. An inherent challenge in hydrodefluorination (HDF) is overcoming the chemical inertness of the C–F σ-bond, whose bond dissociation energy (BDE) can be as great as 130 kcal mol^{-1}.[2] On the other hand, the electron-withdrawing properties of fluorine substituents impart some electron affinity,[3] which makes single-electron transfer (SET) a viable strategy for defluorination, if one can achieve sufficiently negative reduction potentials. Hence, photoredox catalysts, which can harvest the energy from photons to afford highly reducing excited states, represent a potential strategy to achieve hydrodefluorination.

Current reports of photoreductive C–F bond activation are either stoichiometric[4] or require highly activated perfluorinated substrates.[5,6] In 2014, Weaver and co-workers demonstrated HDF of fluorinated arenes using the classic photoredox catalyst, $Ir(ppy)_3$, and Hünig's base as the terminal reductant.[5c] However, the substrate scope was limited to activated perfluoroarenes, such as hexafluorobenzene or pentafluoropyridine.[7] Subsequently, $Ir(ppy)_3$ was shown to hydrodefluorinate trifluoromethylarenes to yield the singly defluorinated CF_2H-substituted arenes.[8] However, the state-of-the-art photoredox catalysts, including both organic and transition-metal based chromophores, typically do not react with fluorobenzene, the simplest aryl fluoride with a BDE of 126 kcal mol^{-1}.[2] One exception is a pyridine-thiolate system that mediates the borylation of relatively inert aryl fluorides; however, the maximal turnovers attained was fewer than three.[9,10]

To expand the substrate scope of transition-metal-based catalysts, judicious modifications of the ligand framework in the $Ir(ppy)_3$ progenitor can boost the overall chemical potential and improve reaction rates. For example, substituting a single ppy ligand with an electron-rich β-diketiminate ligand (NacNac) can increase the excited-state reduction strength by ≈300 to 500 mV (Figure 1).[5a,11] Furthermore, $Ir(ppy)_2$(NacNac) competently dehalogenates various aryl bromides, and aryl chlorides bearing an activating electron-

[*] J. T. Moore,[+] M. J. Dorantes,[+] Z. Pengmei, T. M. Schwartz, J. Schaffner, S. L. Apps, D. A. Blank, C. C. Lu
Department of Chemistry, University of Minnesota, 207 Pleasant Street SE, Minneapolis, Minnesota 55455-0431 (USA)
C. A. Gaggioli, L. Gagliardi
Department of Chemistry, University of Chicago, 5735 S Ellis Ave., Chicago, Illinois 60637 (USA)
T. M. Schwartz, U. Das, C. C. Lu
Institut für Anorganische Chemie, Universität Bonn, Gerhard-Domagk-Str. 1, Bonn 53121, (Deutschland)
E-mail: clu@uni-bonn.de
[+] These authors contributed equally to this work.

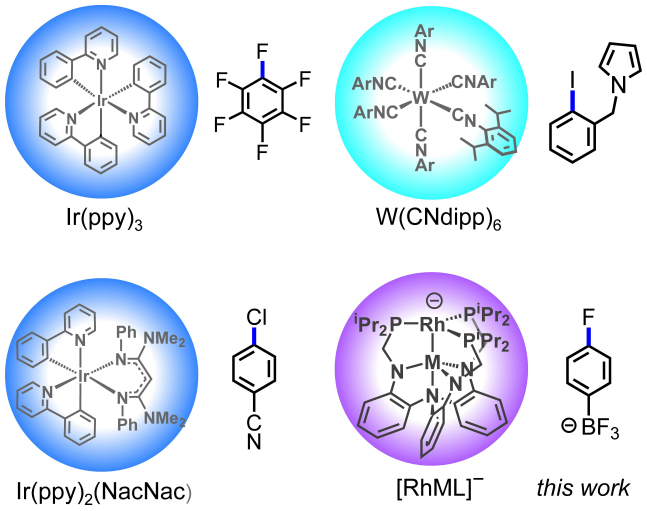

Figure 1. Transition-metal based catalysts that mediate photocatalytic C–X bond activation shown with a representative substrate.[5a,c,12a] The $[RhML]^-$ catalysts are abbreviated as $[\mathbf{1}]^-$, $[\mathbf{2}]^-$, and $[\mathbf{3}]^-$, for M = Al, Ga, and In, respectively. The color of the spheres represents the wavelength of light used in the photoredox catalysis.

withdrawing group.[5a,11] Other non-conventional transition-metal-based chromophores with exceedingly large reducing potentials include $W(CNR)_6$ and a recent isoelectronic Mn^I analogue.[12] However, the substrate scope remains limited to aryl iodides in the former case, and the latter has only demonstrated *trans-to-cis* stilbene isomerization.

Herein, we disclose a distinct class of photoredox catalysts based on the heterobimetallic Rh-group 13 complexes, $[RhM(N(o\text{-}(NCH_2P^iPr_2)C_6H_4)_3)]^-$, which is abbreviated as $[RhML]^-$ where M is Al ($[\mathbf{1}]^-$), Ga ($[\mathbf{2}]^-$), or In($[\mathbf{3}]^-$).[13] The group 13 metalloligands are sigma-acceptors that stabilize low-valent oxidation states at the reactive transition metal center.[14] We previously demonstrated that the supporting metal ion can be varied in a straightforward manner, enabling tuning of the transition metal's ground-state redox potentials, the binding energies of H_2 and N_2, and ultimately, catalytic activity and selectivity.[15] While bifunctional complexes that bond a transition metal to a main-group metalloligand are emerging as versatile catalysts for a broad array of reactions,[16] their known photoinduced reactivity has so far been limited to stoichiometric transformations.[17] In related work, Turro and co-workers have developed dirhodium paddlewheel photocatalysts for H_2 production, which is manageable at relatively low reduction potentials.[18] Herein, we demonstrate that the bifunctional Rh-group 13 complexes are capable photoredox catalysts, and are highly active for the HDF of electron-rich aryl fluorides, which are challenging to reduce via SET. For the most active catalyst $[\mathbf{2}]^-$, irradiation with violet light (λ_{max} 395 nm) engendered the catalytic hydrodefluorination of a variety of substrates, including electron-rich aryl fluorides and trifluoromethylarenes at ambient temperatures in the presence of H_2 and a simple *tert*-butoxide base. Complementary spectroscopic, theoretical, and reactivity studies all support that these anionic Rh-group 13 complexes are powerful photoreductants for catalytic strong aryl–X bond activation.

Results and Discussion

Spectroscopic and Theoretical Study

A combined spectroscopic and theoretical study of the anionic Rh-group 13 complexes, $[\mathbf{1}]^-$, $[\mathbf{2}]^-$, and $[\mathbf{3}]^-$, was conducted. The UV/Vis spectra of the Li salts were collected in THF under Ar (Figure 2a). The solutions of $[\mathbf{1}]^-$, $[\mathbf{2}]^-$, and $[\mathbf{3}]^-$ are all highly colored: purple, teal, and dark green, respectively. Complexes $[\mathbf{2}]^-$ and $[\mathbf{3}]^-$ each exhibit three bands in the visible region, where the λ_{max} of the highest energy peak is at 400 and 413 nm, respectively (Supporting Information, Table S4). The corresponding peak for $[\mathbf{1}]^-$, which is obscured by the ligand-based $\pi\rightarrow\pi^*$ band, was determined to have λ_{max} at 387 nm using a global fit analysis (Figure S14, Table S5). Analogously to the isostructural Ni-group 13 series,[15b] all the absorbances in the visible region gradually red shift as the group 13 support is varied down the periodic table. In a similar trend, the oxidation potentials of the $[RhML]^-$ triad (Figure 2b) become more positive moving from Al (−1.61 V vs. Fc/Fc^+) to Ga (−1.51 V) to In (−1.35 V).[13] Upon addition of 1 atm H_2, all the solutions change color to light yellow as they transform into the corresponding H_2 adducts, $[\mathbf{1\text{-}H_2}]^-$, $[\mathbf{2\text{-}H_2}]^-$, and $[\mathbf{3\text{-}H_2}]^-$.[13] The UV/Vis spectra reveal a single band in the visible region at 381, 397, and 407 nm, respectively (Figure S13). Overall, the relatively high molar absorptivity and minimal energy perturbation upon H_2 binding suggested that irradiation at ≈400 nm may be optimal for photoactivity. Emission spectra for the $[RhML]^-$ complexes were collected under Ar. However, all the complexes were too weakly emissive at room temperature (Figure S19–S23), and no real emission peak was discerned.[4d,19]

Time-dependent density functional theory (TD-DFT) and complete active space self-consistent field (CASSCF) calculations provided insight into the electronic structures of the $[RhML]^-$ complexes and the nature of the electronic transitions (see Supporting Information for details). The ground-state electronic structure is consistent with a sub-valent Rh(−I) center that engages in an "inverse" dative bond to a group 13 σ-acceptor (Figure 2c).[13,20] Notably, five single excitations from doubly filled Rh 4*d* orbitals into the lowest energy molecular orbital (LUMO) were predicted with significant oscillator strengths (Tables S11–S12). Because the LUMOs are similar across the series (Table S10, Figure S29), only that for $[\mathbf{2}]^-$ is described, which has 58 % Rh($5p_z$, $4d_{z^2}$, $5s$), 18 % Ga($4s$, $4p_z$), and 17 % P($3\times4p_z$) contributions (Table S13). Based on good agreement between experimental and theoretical energies (Figure S27), the peak at ≈400 nm is assigned to the Rh($4d_{z^2}$)→LUMO excitation as illustrated by the violet-colored ellipses in Figure 2c. This transition has both Rh→P and intrametal Rh($4d_{z^2}$)→Rh($5p_z$) character that is distinct from the traditional metal-to-ligand charge transfer in $Ru(bpy)_3$ and $Ir(ppy)_3$-type complexes.[11,12b] In addition, the lower energy

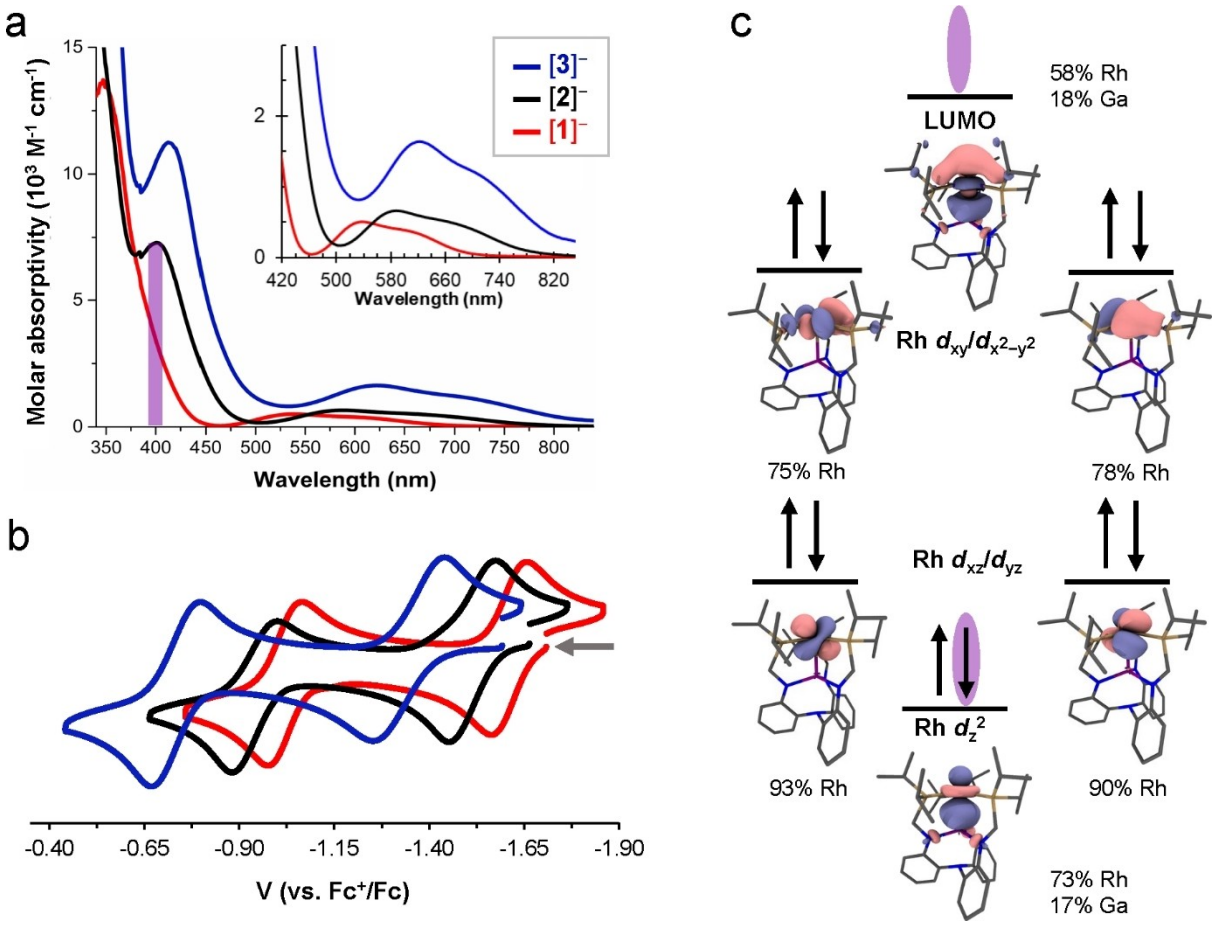

Figure 2. For the $Li(THF)_4$[RhML] complexes, the a) UV/Vis spectra with a zoom of the visible region in the inset; b) cyclic voltammograms in 0.4 M $[N^nBu_4]PF_6$/THF;[13] and c) qualitative MO diagram for $[\mathbf{2}]^-$. See Supporting Information for details.

transitions correspond to the Rh($4d_{x2\text{-}y2}/d_{xy}$)→LUMO and Rh($4d_{xz}/4d_{yz}$)→LUMO excitations (Figure S31–S33).

Hydrodefluorination Catalysis Optimization

In the optimization of the photoredox hydrodefluorination, the substrate *o*-difluorobenzene, *o*-DFB (**4b**), was tested with the Cl-RhML precatalysts,[21] where M is Al (**1-Cl**), Ga (**2-Cl**) and In (**3-Cl**). In a standard run, a J Young NMR tube containing 5 mol % precatalyst, **4b**, 2.5 equiv *tert*-butoxide base, and 4 atm H_2 in THF was irradiated with violet LEDs ($\lambda_{max} = 395$ nm) at ambient temperature (Table S18). The Rh–Al system was discounted early on because **1-Cl** was slow to initiate catalysis; and although the hydride complex **1-H** showed improved activity, it performed poorly relative to the heavier group 13 congeners, **2-Cl** and **3-Cl**.

Next, we compared the group 1 metal ions associated with the *tert*-butoxide base, as well as the addition of a crown-ether encapsulant, such as 15-C-5 and 18-C-6. Across all three Rh-group 13 systems, K^+ gave a higher combined turnover of PhF and PhH than Na^+. The addition of encapsulant (0.1 equiv) also significantly increased the yields of PhH by 50–70 % yield in 48 h (Supporting Information Table S18). Unfortunately, the S_NAr byproducts, *o*-^{t}BuO-F-C_6H_4 and its HDF product PhO^{t}Bu, were also observed for K^+ and K^+/18-C-6, but not for Na^+ or Na^+(15-C-5). It should be noted that KO^{t}Bu is known to be a non-innocent photoreductant that can lead to complex product outcomes.[22] To investigate the potentially non-innocent role of KO^{t}Bu, a control reaction with KO^{t}Bu/18-C-6 in the absence of the Rh catalyst produced 70 % *o*-^{t}BuO-F-C_6H_4, along with minor amounts of PhF (9 %) and PhH (4 %). However, we note that KO^{t}Bu-mediated side-reactivity is less problematic for the electron-rich arylfluorides. Specifically, irradiating KO^{t}Bu/18-C-6 and 4-fluoroanisole (**6d**) resulted in ≤10 % conversion of the substrate after 48 h. Ultimately, by pairing the NaO^{t}Bu with 15-C-5 (0.5 equiv), **2-Cl** gave the best catalyst performance for **4b**, generating PhH in 92(5)% yield with a combined turnover of 38(3). Hence, NaO^{t}Bu/15-C-5 is preferable when substrates are susceptible to S_NAr side reactivity (Figure S36–S44). On the other hand, KO^{t}Bu/18-C-6 is preferable for the electron-rich arylfluorides, such as **6d**.

The top ranking of **2-Cl** in this series presumably stems from the Rh-Ga system striking a careful balance between SET reactivity and stability of the active species. Reactivity

is promoted by more negative reducing potentials in the photoexcited state, whereas stability is linked to less negative potentials in the ground state such that the active species can be efficiently regenerated from H_2 heterolysis (vide infra). Lastly, in a light-dark cycling experiment, we note that yields of PhF/PhH remained stagnant during a 24 h dark period in the middle of the catalytic run (Figure 3). This is consistent with our prior finding that in the absence of irradiation, hydrodefluorination of **4b** by **3-Cl** required heating at 70 °C for 48 h and only formed the partially defluorinated PhF as the major product.

Substrate Scope

Moving forward with **2-Cl**, we first expanded the substrate scope to fluorobenzene (**4a**) and other difluorobenzenes (**4b** to **4e**), as shown in Figure 4a (Table S20, Figure S45–S54). For **4a** to **4e**, photoredox hydrodefluorination was performed using NaO^{t}Bu (1.25 equiv per C–F bond) and 15-C-5 (0.5 equiv per substrate), along with the standard reaction conditions described above. Complete hydrodefluorination proceeded with high yields (89 to 98 %). For **4e**, reaction monitoring by ^{19}F NMR spectroscopy revealed that both F atoms were competitively defluorinated, despite the greater steric congestion of the F atom in the *ortho*-position to the Me substituent. As a stark contrast, under thermal conditions, **4e** was selectively hydrodefluorinated by **3-Cl** to 2-fluorotoluene. [13]

Next, photoredox hydrodefluorination was extended to electron-rich fluoroarenes (**6a** to **6j**, Figures 4b and S55–S75) by using KO^{t}Bu and 18-C-6 with the standard conditions, unless otherwise noted. Good yields were observed for the fluoroarenes with methyl and dimethoxymethyl substituents (**6a** to **6c**). Fluoroarenes with an electron-donating group *para* to the C–F bond (OMe, **6d**; OPh, **6e**; and NMe_2, **6f**) were hydrodefluorinated in high yields (91 to 98 %). Of note, both the reaction yield and the qualitative rate seem to increase with the electron-donating nature of the *para*-substituent: **6a**≈**6c**<**6e**≈**6d**<**6f**. Substrates **6g** and **6h**, which contain multiple methoxy groups adjacent to the C–F bond were converted in high yields (94–95 %) without cleavage of any C–OMe bonds. Boron-based substituents such as pinacolborane (**6i**) or trifluoroborate (**6j**) were also investigated. For **6i**, the desired product, PhBpin, was formed in moderate yield (53 %) alongside unreacted substrate. For the ionic substrate **6j**, which is poorly soluble in THF, the amounts of both 18-C-6 (1.5 equiv) and precatalyst (15 mol %) were increased to achieve 96 % yield of $PhBF_3^-$.

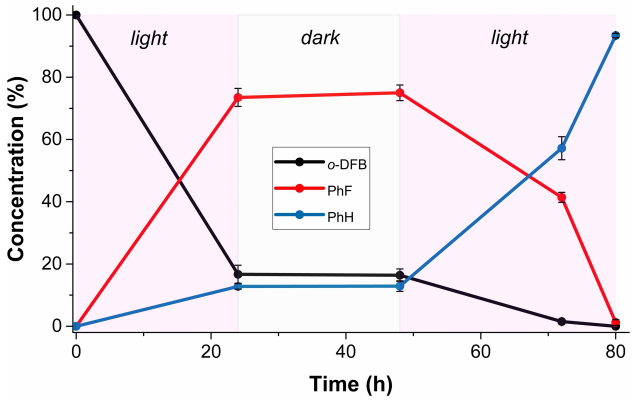

Figure 3. Light-dark cycling experiment for the hydrodefluorination of *o*-DFB using **2-Cl** under standard catalytic conditions.

As shown in Figure 4c, we further probed other types of bond cleavages catalyzed by **2-Cl** under photoredox conditions (Figure S76–S87). Both trifluorotoluene (**8a**) and its 3-fluoro analogue (**8b**) were transformed into toluene in 92 % yield using KO^{t}Bu in the absence of a crown ether. The complete hydrodefluorination of the CF_3 group is noteworthy, as nearly all other photoredox catalysts cleave only a single C–F bond of trifluoromethylarene-type substrates that are typically activated by an electron-withdrawing group.[8,23] Using identical conditions, the C–OCF_3 bond in **8c** was cleaved quantitatively. For **8d**, a substrate that may be susceptible to S_NAr, we used **3-Cl** and NaO^{t}Bu. Cleavage of the benzonitrile group outcompeted cleavage of the C–F bond, with the reaction halting after generating PhF (88 %) and 10 % PhH. We presume the cyanide byproduct poisons the catalyst, precluding complete hydrodefluorination. For the ionic substrate **8e**, increasing the loading of both **2-Cl** (15 mol %) and 18-C-6 (1.5 equiv) resulted in the cleavages of the both C–F and C–SK bonds, resulting in the products, PhSK and PhH, in a 3:2 ratio after 24 h. Additionally, the C(sp^3)–Cl bond in 1-chloroadamantane (**8f**) was cleanly hydrodechlorinated using 5 mol % **2-Cl** and 0.5 equiv 18-C-6.

Complex substrates featuring additional functional groups were then targeted (Figure 5). *N*-Methyl paroxetine (**10a**), a benzodioxole that is a derivative of the antidepressant paroxetine, was defluorinated using the standard conditions with KO^{t}Bu and 18-C-6. Reaction monitoring via NMR spectroscopy showed clean defluorination in a high yield of 97 % across triplicate runs (Figure S108–S109). Because the product was amenable to isolation, we then tested a preparatory-scale defluorination with 910 μmol of **10a** (see Supporting Information for details). After an irradiation period of 72 h, the defluorinated product was isolated as a pale-yellow oil in 70 % yield via purification by column chromatography (Figure S110–S111). Flurbiprofen (**10b**), a nonsteroidal anti-inflammatory drug, was also subjected to photocatalytic defluorination on preparatory scale under essentially identical conditions, except that an additional equiv KO^{t}Bu was needed because of the carboxylic acid functionality. After an acidic work-up and purification by column chromatography, the defluorinated product of **10b** was isolated as a white solid in 60 % yield (Figure S112–S113). It is notable that the photocatalytic conditions can tolerate the unprotected carboxylic acid.

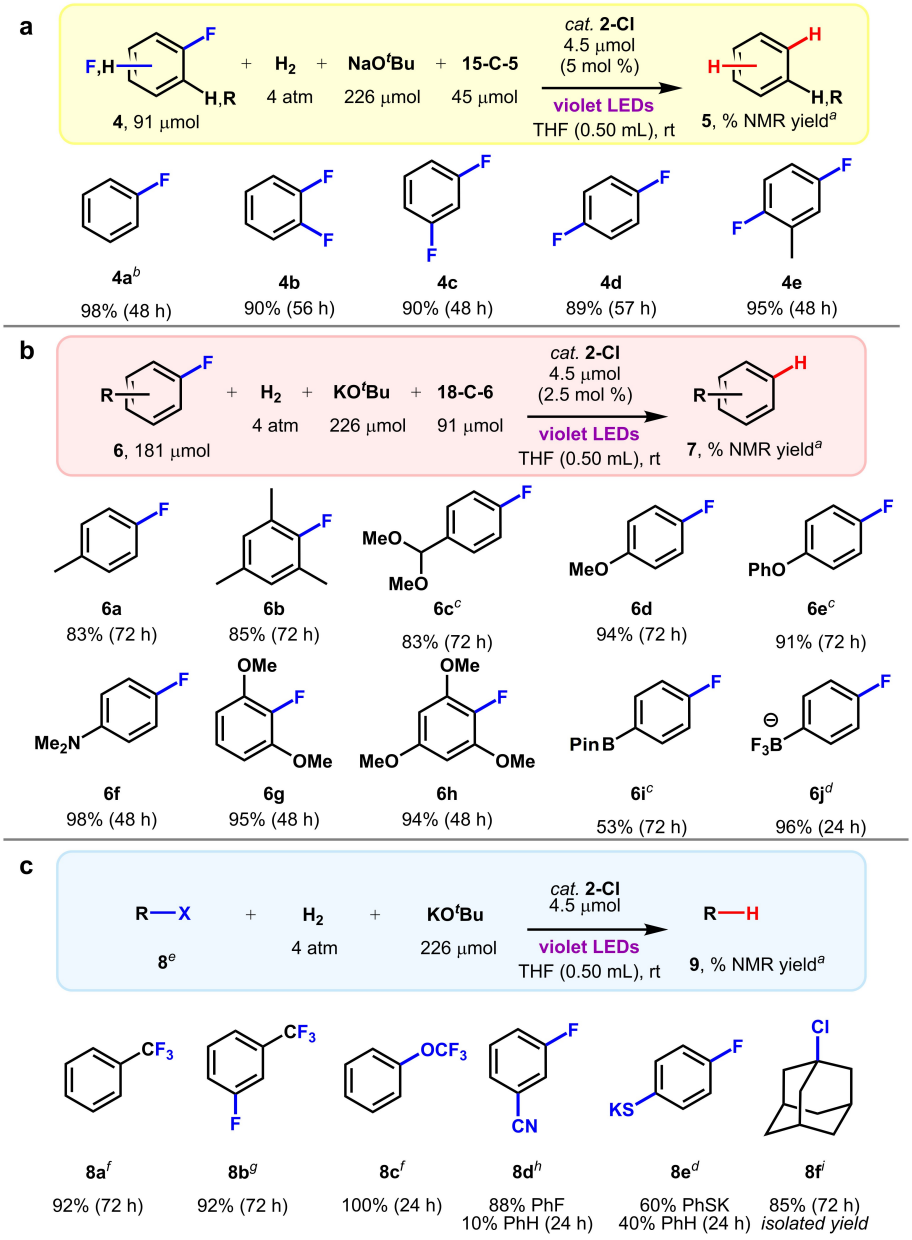

Figure 4. Substrate scope for a,b) the hydrodefluorination of aryl fluorides and c) other C–X bond activations using **2-Cl** and standard catalytic conditions unless otherwise specified. Footnotes: [a] Triplicate runs. Yield based on ^{1}H NMR integration of product relative to that of a NaB(ArF)$_4$ in THF as a sealed capillary. [b] **4a** (181 μmol), 15-C-5 (91 μmol), catalyst (2.5 mol%). [c] No 18-C-6. [d] Due to poor solubility: K[**6j**] and **8e** (30.1 μmol), KO^{t}Bu (37.7 μmol), 18-C-6 (45.2 μmol), catalyst (15 mol%). [e] The catalyst loading is 2.5 mol% unless otherwise specified. [f] 7.5 mol% catalyst. [g] 10.0 mol% catalyst. [h] Using NaO^{t}Bu and **3-Cl**. [i] **8f** (181 μmol), 18-C-6 (91 μmol).

Mechanistic Studies

Figure 6 depicts the proposed catalytic cycle for the photoredox hydrodefluorination of fluorobenzene starting from **2-Cl**. Previously, we showed that the Cl-RhML complexes are converted into [(η^2-H$_2$)RhML]$^-$ after two consecutive H$_2$-binding and deprotonation events.[13] The first H$_2$ heterolysis initiates the catalytic cycle by forming **2-H**, while the second heterolysis leads to a putative Rh^I dihydride that reductively eliminates H$_2$ to form the formally reduced Rh(–I) species, [**2-H$_2$**]$^-$.[13] Next, we envision the dissociation of H$_2$ followed by photoexcitation to generate the excited complex [**2**]$^-$*, which then engages in SET to the fluoroarene to provide the oxidized Rh^0 species **2^{ox}** and the fluorinated radical anion. The latter then undergoes F$^-$ mesolytic dissociation to form a highly reactive aryl radical (Ph–H BDE = 112.8 kcal mol^{-1}), which is intercepted by H-atom transfer from the THF solvent (BDE = 92 kcal mol^{-1}).[2] Complex **2^{ox}** then undergoes a binuclear oxidative addition of H$_2$ to regenerate **2-H**, which closes the catalytic cycle.

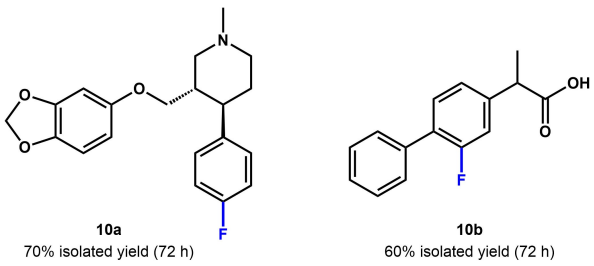

Figure 5. Preparatory-scale hydrodefluorination of complex aryl fluorides **10a** and **10b** (910 μmol) with 2.5 mol% **2-Cl**, 4 atm H_2, KO^{t}Bu (1.25 to 2.25 equiv), and 18-C-6 (0.5 equiv).

The later steps in the photoredox cycle are supported by stoichiometric and isotope labeling experiments. Stoichiometric hydrodefluorination reactions between K(THF)$_x$[**2**] and *o*-DFB produced PhF in good yields when irradiated under Ar in THF, thereby demonstrating that SET does not require H_2 or alkoxide base to proceed (Table S21, Figure S89–S90). While the viability of K(THF)$_x$[**2**] implicates [RhML]$^-$* as the active species in SET, we cannot rule out the activity of [(η^2-H_2)RhML]$^-$ or whether photon absorption is accompanied by H_2 dissociation in the excited state. The SET to the substrate is consistent with the increased rates of hydrodefluorination for electron-rich fluoroarenes, as previously, aryl chlorides with more electron-donating groups exhibited faster rates of Cl^- dissociation upon one-electron reduction.[24] Catalytic isotope labeling studies with *o*-DFB, 2.5 equiv NaO^{t}Bu, and 5 mol% **3-Cl** showed minimal deuterium incorporation in the PhF product when employing D_2 in protio-THF (8.5% at 48 h, Figure S95–S98, Table S22). On the other hand, deuterium incorporation in the product became significant (88%) when the reaction was performed with H_2 in THF-d_8. Moreover, the ^{2}H NMR spectrum of the former reaction revealed significant deuterium incorporation at the α C–H of protio-THF. These results evidence the primary role of H_2 as a reductant and confirm THF as the primary H-source for the product's C–H bond. Notably, these findings contrast with that observed for the dark hydrodefluorination reaction of *o*-DFB catalyzed by **3-Cl**, where deuterium incorporation occurs largely from D_2 (86%, 70 °C).[13] Finally, complex **2^{ox}** when exposed to 4 atm H_2 converts readily into **2-H** without irradiation, though a slightly accelerated rate was observed with irradiation (Figure S91).

Zero-valent Rh complexes are rare,[25] and the Rh^0 metalloradical **2^{ox}** is a new intermediate that has not yet been characterized. We independently prepared **2^{ox}**, as well as the Al congener, RhAlL (**1^{ox}**), by mixing equal equivalents of Cl-RhML with its reduced counterpart, K(THF)$_x$-[RhML]. The solid-state structure of **1^{ox}** (Figure 7a, Tables S1 and S9) features a Rh–Al bond length of 2.4736(5) Å that is consistent with the presence of a metal-metal interaction and is between that measured for Rh^I **1-H** and Rh(–I) K(THF)$_3$[**1**] at 2.4974(14) and 2.4088(9) Å, respectively.[13,21] The correlation between bond length and the Rh oxidation state supports an inverse dative Rh→M bond, where the Rh metal donates electron density to the Lewis-acidic σ-acceptor M. The solid-state structure of **1^{ox}** reveals a four-coordinate Rh center that is significantly distorted from C_3-symmetry, as reflected by one large P3–Rh–P1 bond angle as well as one elongated Rh–P1 bond. The structural perturbation is consistent with a Jahn–Teller distortion arising from the Rh^0 electronic structure where a single electron populates one of the degenerate Rh d_{xy}/d_{x2-y2} orbitals. The X-band EPR spectra of **1^{ox}** and **2^{ox}** confirm the $S=1/2$ spin states (Figure 7b; Figure S8–S9). Since the spectra are similar, only that for **2^{ox}** will be discussed. At 30 K, the EPR spectrum of **2^{ox}** in frozen toluene features a pseudo axial signal with $g=(2.17, 2.03, 2.01)$, where g_{avg} is 2.07. Hyperfine coupling to ^{103}Rh ($I=1/2$, 100% abundant) was fitted using A values of (7, 454, 437) MHz, which is significantly larger than that measured for other Rh^0 species (Table S24).[25] Indeed, the calculated spin densities of **1^{ox}** and **2^{ox}** show that a large fraction of the

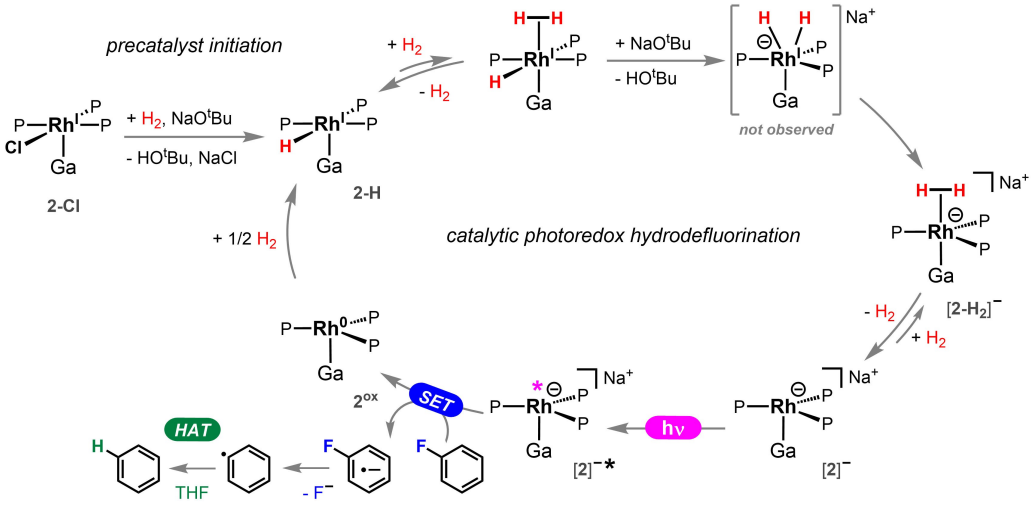

Figure 6. Proposed cycle for the catalytic photoredox hydrodefluorination of fluorobenzene by **2-Cl** in THF.

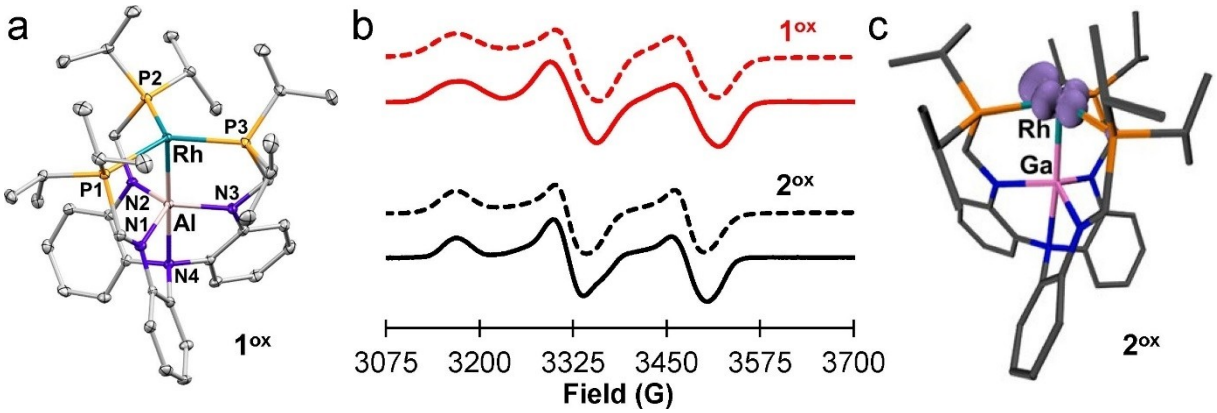

Figure 7. a) Solid-state structure of RhAlL, **1^{ox}**, shown at 50% probability level. H atoms and solvent molecules are omitted for clarity. Selected bond lengths (Å) and angles (°): Rh–Al, 2.4736(5); Rh–P1, 2.3407(5); Rh–P2, 2.2830(4); Rh–P3, 2.2956(4); P1–Rh–P2, 111.089(16); P2–Rh–P3, 107.974(16); P3–Rh–P1, 138.755(17). b) X-band EPR spectra (9.65 GHz, 10 G modulation amplitude, solid line) and simulations (dashed lines) of **1^{ox}** (30 K, 200 μW) and **2^{ox}** (30 K, 635 μW) as frozen toluene (2 mM) samples. c) Spin density plot of **2^{ox}**, shown at an isovalue of 0.01.

unpaired spin (≈60%) resides on Rh (Figure 7c; Figure S34 and Table S17). Of note, the reaction between K(THF)$_x$[**2**] and C_6D_5F in THF-d_8 after 12 h irradiation generated C_6D_6, **2^{ox}**, and *protio*-**2-H** (Figs. S99–S107). While the formation of C_6D_6 and **2^{ox}** is consistent with SET, the appearance of **2-H** may seem problematic given that the H-atom source must either be the ligand or the glass reaction vessel. However, we note that this side reaction should not interfere with catalysis because **2^{ox}** is readily intercepted by H_2 to form **2-H**, turning over the catalytic cycle. The latter reaction occurs readily and cleanly in the dark, and is only slightly accelerated by irradiation (Figure S91).

Conclusion

A new strategy for photoredox catalysis is presented based on a heterobimetallic Rh-group 13 core. The group 13 σ-acceptor serves both to stabilize the formally anionic Rh(–I) center in the ground state and to lower the Rh($5p_z$)-based LUMO, which is well poised for photon-induced SET. The complex $[RhGaL]^-$ is a powerful photoreductant, catalyzing the hydrodefluorination of electron-rich aryl fluorides, including some anionic derivatives, and trifluoromethylarenes at ambient temperature with violet-light irradiation. The catalyst system operates under an unusual mechanism that turns over with H_2 and a simple alkoxide base as the terminal reductant, though HAT also occurs from the THF solvent. Extension to other C(sp^2)–X bond cleavages was demonstrated for X = CN, S^-, and OCF_3, as well as the C(sp^3)–Cl bond in adamantyl chloride. In support of the SET mechanism, a Rh^0 intermediate was spectroscopically and structurally characterized.

Supporting Information

The Supporting Information is available free of charge at X-ray crystallographic data for **1^{ox}** (CIF) XYZ coordinates of calculated structures (XYZ) Experimental procedures, characterizations, spectroscopic data, computational methods, and theoretical data (PDF)

Acknowledgements

This material is based upon work supported by the National Science Foundation under Grant Nos. 2102095 and 2054723. We thank Dr. Andrew Healy, Prof. Aaron Massari, Connor Reilly, and Dr. Victor Young, Jr. for experimental assistance. TMS, UD, and CCL gratefully acknowledge Prof. Alexander Filippou for providing access to facilities and additional resources.

Conflict of Interest

The authors declare no conflict of interest.

Data Availability Statement

The data that support the findings of this study are available in the supplementary material of this article.

Keywords: Gallium · Heterobimetallic · Hydrodefluorination · Photoredox Catalysis · Rhodium

[1] a) J. Wang, M. Sanchez-Rosello, J. L. Acena, C. del Pozo, A. E. Sorochinsky, S. Fustero, V. A. Soloshonok, H. Liu, *Chem. Rev.* **2014**, *114*, 2432–2506; b) M. Inoue, Y. Sumii, N. Shibata, *ACS Omega* **2020**, *5*, 10633–10640; c) T. Fujiwara, D. O'Hagan, *J. Fluorine Chem.* **2014**, *167*, 16–29.
[2] Y. R. Luo, *Comprehensive Handbook of Chemical Bond Energies*, 1st ed., CRC Press, Boca Raton, FL, **2007**; p. 211.
[3] K. S. Gant, L. G. Christophorou, *J. Chem. Phys.* **1976**, *65*, 2977–2981.

[4] a) A. M. Mfuh, J. D. Doyle, B. Chhetri, H. D. Arman, O. V. Larionov, *J. Am. Chem. Soc.* **2016**, *138*, 2985–2988; b) L. Zhang, L. Jiao, *J. Am. Chem. Soc.* **2019**, *141*, 9124–9128; c) J. Qin, S. Zhu, L. Chu, *Organometallics* **2021**, *40*, 2246–2252; d) F. Glaser, C. B. Larsen, C. Kerzig, O. S. Wenger, *Photochem. Photobiol. Sci.* **2020**, *19*, 1035–1041.

[5] a) J. H. Shon, D. Kim, M. D. Rathnayake, S. Sittel, J. Weaver, T. S. Teets, *Chem. Sci.* **2021**, *12*, 4069–4078; b) A. Singh, J. J. Kubik, J. D. Weaver, *Chem. Sci.* **2015**, *6*, 7206–7212; c) S. M. Senaweera, A. Singh, J. D. Weaver, *J. Am. Chem. Soc.* **2014**, *136*, 3002–3005; d) J. I. Day, S. Grotjahn, S. Senaweera, B. Koenig, J. D. Weaver Iii, *J. Org. Chem.* **2021**, *86*, 7928–7945; e) J. Lu, N. S. Khetrapal, J. A. Johnson, X. C. Zeng, J. Zhang, *J. Am. Chem. Soc.* **2016**, *138*, 15805–15808; f) J. Burdeniuc, R. H. Crabtree, *J. Am. Chem. Soc.* **1996**, *118*, 2525–2526.

[6] Z. Wang, Y. Sun, L.-Y. Shen, W.-C. Yang, F. Meng, P. Li, *Org. Chem. Front.* **2022**, *9*, 853–873.

[7] C. Cavedon, P. H. Seeberger, B. Pieber, *Eur. J. Org. Chem.* **2019**, 1379–1392.

[8] K. Chen, N. Berg, R. Gschwind, B. Konig, *J. Am. Chem. Soc.* **2017**, *139*, 18444–18447.

[9] a) S. Wang, H. Wang, B. König, *Chem* **2021**, *7*, 1653–1665; b) S. Wang, H. Wang, B. Konig, *J. Am. Chem. Soc.* **2021**, *143*, 15530–15537.

[10] For other exceptions, see: a) V. A. Pistritto, M. E. Schutzbach-Horton, D. A. Nicewicz, *J. Am. Chem. Soc.* **2020**, *142*, 17187–17194; b) Y.-M. Tian, X.-N. Guo, M. W. Kuntze-Fechner, I. Krummenacher, H. Braunschweig, U. Radius, A. Steffen, T. B. Marder, *J. Am. Chem. Soc.* **2018**, *140*, 17612–17623.

[11] J.-H. Shon, S. Sittel, T. S. Teets, *ACS Catal.* **2019**, *9*, 8646–8658.

[12] a) J. Fajardo Jr., A. T. Barth, M. Morales, M. K. Takase, J. R. Winkler, H. B. Gray, *J. Am. Chem. Soc.* **2021**, *143*, 19389–19398; b) W. Sattler, L. M. Henling, J. R. Winkler, H. B. Gray, *J. Am. Chem. Soc.* **2015**, *137*, 1198–1205; c) P. Herr, C. Kerzig, C. B. Larsen, D. Haussinger, O. S. Wenger, *Nat. Chem.* **2021**, *13*, 956–962; d) C. Wegeberg, O. S. Wenger, *Dalton Trans.* **2022**, *51*, 1297–1302.

[13] J. T. Moore, C. C. Lu, *J. Am. Chem. Soc.* **2020**, *142*, 11641–11646.

[14] a) G. Parkin, *Organometallics* **2006**, *25*, 4744–4747; b) A. Amgoune, D. Bourissou, *Chem. Commun.* **2011**, *47*, 859–871; c) P. A. Rudd, S. Liu, L. Gagliardi, V. G. Young Jr., C. C. Lu, *J. Am. Chem. Soc.* **2011**, *133*, 20724–20727.

[15] a) B. L. Ramirez, C. C. Lu, *J. Am. Chem. Soc.* **2020**, *142*, 5396–5407; b) R. C. Cammarota, J. Xie, S. A. Burgess, M. V. Vollmer, K. D. Vogiatzis, J. Ye, J. C. Linehan, A. M. Appel, C. Hoffmann, X. Wang, V. G. Young Jr., C. C. Lu, *Chem. Sci.* **2019**, *10*, 7029–7042; c) S. P. Desai, J. Ye, J. Zheng, M. S. Ferrandon, T. E. Webber, A. E. Platero-Prats, J. Duan, P. Garcia-Holley, D. M. Camaioni, K. W. Chapman, M. Delferro, O. K. Farha, J. L. Fulton, L. Gagliardi, J. A. Lercher, R. L. Penn, A. Stein, C. C. Lu, *J. Am. Chem. Soc.* **2018**, *140*, 15309–15318; d) R. C. Cammarota, M. V. Vollmer, J. Xie, J. Ye, J. C. Linehan, S. A. Burgess, A. M. Appel, L. Gagliardi, C. C. Lu, *J. Am. Chem. Soc.* **2017**, *139*, 14244–14250.

[16] a) J. Takaya, *Chem. Sci.* **2021**, *12*, 1964–1981; b) D. You, F. P. Gabbaï, *Trends Chem.* **2019**, *1*, 485–496; c) G. Bouhadir, D. Bourissou, *Chem. Soc. Rev.* **2016**, *45*, 1065–1079.

[17] a) T. P. Lin, F. P. Gabbai, *J. Am. Chem. Soc.* **2012**, *134*, 12230–12238; b) S. Sahu, F. P. Gabbai, *J. Am. Chem. Soc.* **2017**, *139*, 5035–5038; c) M. Karimi, E. S. Tabei, R. Fayad, M. R. Saber, E. O. Danilov, C. Jones, F. N. Castellano, F. P. Gabbai, *Angew. Chem. Int. Ed.* **2021**, *60*, 22352–22358; *Angew. Chem.* **2021**, *133*, 22526–22532.

[18] a) S. Lin, C. Turro, *Chem. Eur. J.* **2021**, *27*, 5379–5387; b) T. J. Whittemore, H. J. Sayre, C. Xue, T. A. White, J. C. Gallucci, C. Turro, *J. Am. Chem. Soc.* **2017**, *139*, 14724–14732.

[19] J.-H. Shon, T. S. Teets, *Comments Inorg. Chem.* **2020**, *40*, 53–85.

[20] M. V. Vollmer, J. Ye, J. C. Linehan, B. J. Graziano, A. Preston, E. S. Wiedner, C. C. Lu, *ACS Catal.* **2020**, *10*, 2459–2470.

[21] J. T. Moore, N. E. Smith, C. C. Lu, *Dalton Trans.* **2017**, *46*, 5689–5701.

[22] S. Yanagisawa, K. Ueda, T. Taniguchi, K. Itami, *Org. Lett.* **2008**, *10*, 4673–4676.

[23] a) D. B. Vogt, C. P. Seath, H. Wang, N. T. Jui, *J. Am. Chem. Soc.* **2019**, *141*, 13203–13211; b) J. B. I. Sap, N. J. W. Straathof, T. Knauber, C. F. Meyer, M. Medebielle, L. Buglioni, C. Genicot, A. A. Trabanco, T. Noel, C. W. Am Ende, V. Gouverneur, *J. Am. Chem. Soc.* **2020**, *142*, 9181–9187; c) F. Wang, Y. Nishimoto, M. Yasuda, *J. Am. Chem. Soc.* **2021**, *143*, 20616–20621.

[24] C. Costentin, M. Robert, J. M. Saveant, *J. Am. Chem. Soc.* **2004**, *126*, 16051–16057.

[25] a) P. J. Nance, N. B. Thompson, P. H. Oyala, J. C. Peters, *Angew. Chem. Int. Ed.* **2019**, *58*, 6220–6224; *Angew. Chem.* **2019**, *131*, 6286–6290; b) B. de Bruin, J. C. Russcher, H. Grützmacher, *J. Organomet. Chem.* **2007**, *692*, 3167–3173; c) S. Deblon, L. Liesum, J. Harmer, H. Schönberg, A. Schweiger, H. Grützmacher, *Chem. Eur. J.* **2002**, *8*, 601–611; d) B. Longato, R. Coppo, G. Pilloni, C. Corvaja, A. Toffoletti, G. Bandoli, *J. Organomet. Chem.* **2001**, *637–639*, 710–718; e) J. H. B. Chenier, M. Histed, J. A. Howard, H. A. Joly, H. Morris, B. Mile, *Inorg. Chem.* **1989**, *28*, 4114–4119; f) G. N. George, S. I. Klein, J. F. Nixon, *Chem. Phys. Lett.* **1984**, *108*, 627–630.

[26] Deposition number 2098279 (for **1^{ox}**) contains the supplementary crystallographic data for this paper. These data are provided free of charge by the joint Cambridge Crystallographic Data Centre and Fachinformationszentrum Karlsruhe Access Structures service.

Manuscript received: April 15, 2022
Accepted manuscript online: August 26, 2022
Version of record online: September 14, 2022